CFD MODELING OF POROUS MEDIA IN THE STUDY OF THE FLOW AT PENSTOCK INTAKE OF A 1:30 MODEL OF GURI HYDRO-POWERHOUSE

Arevalo, Angela
angelagau@gmail.com
Graduate Student, Mechanical Engineering. Universidad Simón Bolívar

Montilla, Gonzalo
gmontilla@edelca.com.ve
CVG-EDELCA. Dpto. de Hidráulica, Complejo Hidroeléctrico Macagua, Edo. Bolívar, Venezuela

Rojas-Solórzano, Luis
rrojas@usb.ve
Dpto. de Conversión de Energía, Edif. ENE, Universidad Simón Bolívar, Caracas,Venezuela

Reyes, Miguel
mareyes@usb.ve
Dpto. de Termodinámica, Edif. ENE, Universidad Simón Bolívar, Caracas,Venezuela

Marín, Juan
jcmm_cemfa@yahoo.com
Center for Fluid Mechanics (CEMFA). Universidad Simón Bolívar

ABSTRACT

The transient free surface flow within a 1:30 model of the intake (penstock) to Power House II of Guri Hydro-Power Plant (Venezuela) is studied. The geometry of the model includes a reservoir of 4.31 meters upstream the dam.
Geometric details and appropriate boundary conditions were reproduced mathematical and numerically using CFD (Computational Fluid Dynamics) techniques, running the commercial code CFX^{TM} 4.4. The flow features nearby and within the penstock were captured. Special attention was paid to the evaluation of air entrainment that might eventually form due to the presence of free surface vortices.
The computational domain included the anti-debris screen at the entrance of the penstock, considering it as a porous medium with equivalent permeability and porosity.
Most of simulated cases corresponded to conditions in the prototype Guri´s free surface level of 240 a.s.l. (above sea level), with flow rate of 450 m^3/seg. Air and water were considered incompressible fluids with and homogeneous interfacial transport model. Computed velocity profiles at different sections of the reservoir and pressure head along the penstock are compared with experiments. The numerical model captures the influence of the porous medium, used to simulate the anti-debris grill, onto the free-surface and pressure head within the penstock.
In order to improve the predictive capabilities of the numerical model and to diminish the instabilities caused by the hydrostatic pressure condition at the entrance of the computational reservoir, preliminary results including a porous wall at the upstream boundary are presented. The porous wall, in fact, mimics the water-calming rock wall placed at the entrance of the experimental reservoir and proved to be a relevant element in improving the CFD predictions.

INTRODUCTION

The generation of the huge hydro-electrical capacity of the Caroní River is under the responsibility of the Corporación Venezolana de Guayana (CVG) through its subsidiary Electrificación del Caroní (EDELCA). In fact, the hydro-electrical potential of the Caroní River, in the South of Venezuela, represents the most important water resource of the country. This resource has permitted the industrial take-off of Ciudad Guayana

and the electrification of most of the country. Currently, there are three hydroelectrical power complexes along the Caroní River: Macagua, Guri and Caruachi, while there is one more in construction: Tocoma. The Guri hydro-electrical complex, the largest of them (and the third largest in the world), generates 10000MW, more than the 50% of the electric power of Venezuela.
The strong dry season on the Caroní basin between years 2000 and 2003, caused a dramatic level drop of Guri´s reservoir. The study of the impact of those low and potentially even lower levels of Guri´s reservoir motivated CVG-EDELCA´s Hydraulics Laboratory to build a not-distorted 1:30 scale model of Guri´s dam and turbine penstock, for the expected most critical unit (which is located in Power House II). In this model numerous trials have been carry out to study the operation of the turbines with low falls. Although the experimental facility helped exploring a vast range of flows and free-surface levels, this numerical study focused on the evaluation of the porous medium as an appropriate model for the anti-debris grill and rock wall; therefore, the numerical study presents and compares the performance of the CFD model for the design flow condition (equivalent prototype flow rate of Qp = 450 m^3/seg) and the minimum allowed design elevation (equivalent prototype elevation of 240 a. s. l.) with experiments.

PHYSICAL MODEL
This work compares numerical results to experiments on a reduced-scale physical model. The physical model was chosen such that it satisfies geometric and Froude similarity with the prototype (Montilla, 2004). As usual, the large flow inertia in the problem permits the distorted Reynolds not to be an issue of concern.

MATHEMATICAL MODEL
The modeling and mathematical analysis are developed on the commercial program ANSYS-CFX4.4^{TM}. One of the biggest challenges in the simulation of the hydraulic model was to model the anti-debris grill at the penstock entrance. Because of the actual grill complex geometry it would be prohibitive to develop a one-to-one computational geometry; therefore, a porous medium was proposed instead, with equivalent permeability and porosity as those existing in the scale model grill. Another difficulty was presented at the entrance of the computational reservoir, since the hydrostatic pressure boundary condition behaves very unstable and further treatment is needed in order to comply with the actual flow approaching features. Figure 1 depicts the geometry of the computational model.

Boundary Conditions
A hydrostatic pressure condition was preset at the reservoir entrance, such that it leads to the desired free-surface level. The top of the computational domain (both reservoir and sluice gates upper side) was set open to atmosphere. A constant velocity profile, according to the operating flow-rate, was set at the penstock discharge (hypothetically towards the turbine). All boundary conditions are shown in Fig. 1.

CFD MODELING
CFD is a computational technique for the numerical solution of the time and spatially discrete fluid mechanics governing equations. In this work, the simulations are carried out on CFX4.4^{TM}, a commercial open CFD code, which is designed and validated for computing the flow field by using the finite control volume technique.

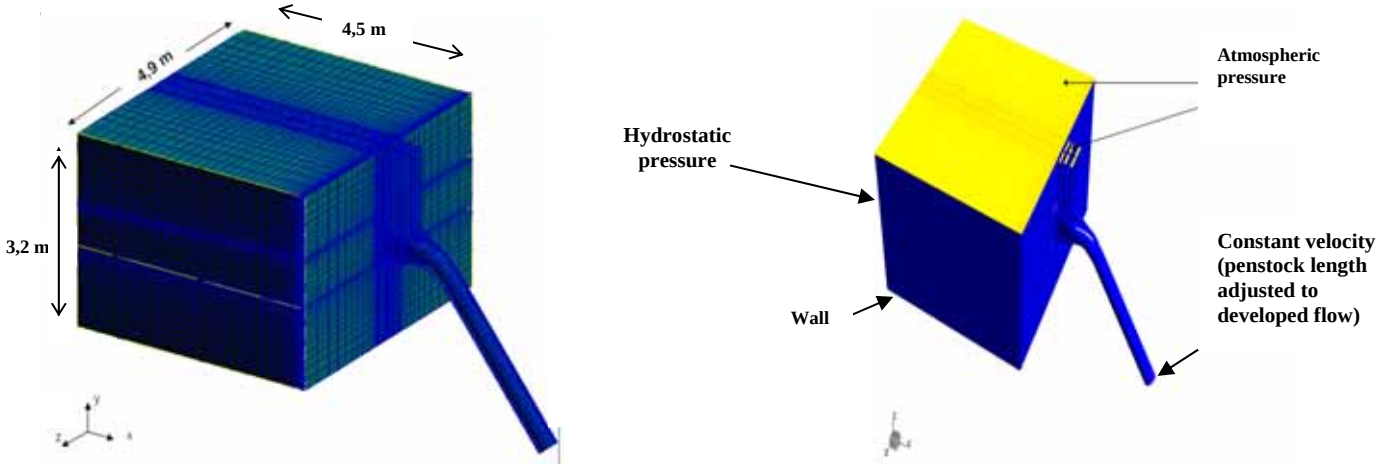

Fig.1 Computational Model and boundary conditions

Numerical Issues

The numerical method works by dividing the physical region into a large number of control volumes (AEA Technology, 1997). The set of differential governing equations are written as algebraic equations within each of those control volumes, after applying finite differences to relate the pressure, velocity and other variables (e.g., volumetric fraction) with values in neighbor volumes. The solution to the problem consists in the solution of a non-linear system of algebraic equations.

The control volume method divides the domain in a large number of control volumes with a central node and, in general, it is connected to neighboring control volumes.

All the terms in the governing equations, except the convective term, are spatially discretized using second order central differences. A hybrid scheme is used to discretize the convective term. The non-linear nature of the governing equations leads to an iterative solution procedure of the system of equations. The pressure term is dealt as a source term in the momentum equation and the SIMPLEC (Patankar, 1983) algorithm is used to couple the mass and momentum equations. This semi-implicit algorithm solves the continuity equation through a pressure correction term for the velocity components. Further details are presented in AEA Technology (1997).

Free Surface Air-Water Homogeneous Modeling

First, the turbulence is modeled using the Reynolds Averaged Navier-Stokes (RANS) and mass equations and the two-equation model based on the turbulent viscosity and the turbulent kinetic energy 'k' and turbulent dissipation 'ε', named the k- ε model with wall functions (AEA Technology, 1997).

To model the air-water segregated flow, the mass conservation of each phase is solved as one of the set of governing equations, while the momentum equation (RANS) for each phase are added up to get rid of the interphase momentum transfer. There is a closure equation for the volume fraction, which states that both phases volume fraction must add up to one at every fluid location.

The homogeneous multiphase model considers the possibility of air-water mixture, at a larger scale than molecular, while still at smaller scale than what is being solved for. This is, each phase is treated as an inter-penetrating continuum, which implies that each phase may be present in every control volume and, the phase volume fraction is equal to the fraction of volume occupied. Therefore, the problem is solved in an Eulerian-Eulerian frame of reference for the two phases, even though the intrinsic volumetric forces (e.g., gravity) will determine, through mass conservation, the solely existence, co-existence or non-existence of a single phase.

Both phases are considered to be incompressible and isothermal.

Therefore, the governing equations are presented, indicating with the sub-index each phase, as follows:

Mass Conservation:

$$\nabla \bullet \left(r_\alpha \rho_\alpha U_\alpha \right) = 0 \tag{1}$$

RANS:

$$\frac{\partial}{\partial t}(\rho U) + \nabla \bullet \left(\left(\rho U \otimes U - \mu \left(\nabla U + (\nabla U)^T \right) \right) \right) = \left(B - \nabla p \right) \tag{2}$$

In eqn. (2), the left-hand-side terms represent the transport of convective and diffusive momentum. The right-hand-side term represents the body and pressure forces.
Furthermore, in this equation:

$$U_\alpha = U_\beta = U \tag{3}$$

$$p_\alpha = p_\beta = p \tag{4}$$

$$\rho = \sum_{\alpha=1}^{2} r_\alpha \rho_\alpha \tag{5}$$

$$\mu = \sum_{\alpha=1}^{Np} r_\alpha \mu_\alpha \tag{6}$$

And the algebraic restriction for all volume fractions at each control volume:

$$\sum_{\alpha=1}^{2} r_\alpha = 1 \tag{7}$$

The multiphase model here proposed has proven to give a good approximation (i.e., CRS4 Technical Report 99/20, 1999) when the gravity force trends to stratify the phases as in free surface flows. In this case, the volume fractions are equal to 1 or 0 everywhere, except at the interphase, which makes it reasonable to have a unique velocity field for both phases.

Interphase Refinement Algorithm

During the simulation convergence iterative process, the water and air, initially mixed, tend to segregate due to their differences in density, creating homogeneous volume fraction fields for each phase, equal to 0 or to 1, such that it suddenly changes at the two-fluid interphase. To avoid a blurry interphase caused by numerical diffusion of the volumetric fraction equations (mass conservation for each phase), a refinement algorithm is used. This surface contouring algorithm requires a local fine mesh and therefore a proficient user-analyst.
In detail, the algorithm adjusts the volumetric fraction of the fluids at the interphase for each iteration. The interphase is defined as the surface in which volume fraction for both fluids, r_1 and r_2, are equal to 0.5 each. Firstly, the program identifies the control volumes at the interphase, by checking whether or not r_1-0.5 for certain control volume changes sign with respect to its neighbors. Then, the program identifies the fluid on the wrong side of the interphase and translates it to the right side, ensuring the volume conservation. During this procedure, all the interphase volumes are fixed.

Turbulent Model

The two-equation model used in these simulations is the standard k-ε with wall functions for dampening the turbulent viscosity near the walls. The equations of the model are:
Transport of Turbulent Kinetic Energy k :

$$\nabla \bullet \left(r_\alpha \left(\rho_\alpha U_\alpha k_\alpha - \left(\mu + \frac{\mu_{T\alpha}}{\sigma_k} \right) \nabla k_\alpha \right) \right) = r_\alpha S_{k\alpha} \tag{8}$$

Transport of the Dissipation Rate of Turbulent Kinetic Energy ε :

$$\nabla \bullet \left(r_\alpha \left(\rho_\alpha U_\alpha \varepsilon_\alpha - \left(\mu + \frac{\mu_{T\alpha}}{\sigma_\varepsilon} \right) \nabla \varepsilon_\alpha \right) \right) = r_\alpha S_{\varepsilon\alpha} \tag{9}$$

Where the respective source terms are given by:

$$S_{k\alpha} = P_\alpha + G_\alpha - \rho_\alpha \varepsilon_\alpha \tag{10}$$

$$S_{\varepsilon\alpha} = \frac{\varepsilon_\alpha}{k_\alpha}\left(C_{1\varepsilon}\left(P_\alpha + C_{3\varepsilon} max\left(G_\alpha, 0\right)\right) - C_{2\varepsilon}\rho_\alpha \varepsilon_\alpha\right) \tag{11}$$

The turbulent viscosity is calculated through the Prandtl-Kolmogorov relationship:

$$\mu_{T\alpha} = C_\mu \rho_\alpha \frac{k_\alpha^2}{\varepsilon_\alpha} \tag{12}$$

and the empirical coefficients (taken for free turbulence cases) given by: C_μ=0.09; C_1=1.44; C_2=1.92; C_3=0.0; and C_k=0.4187.

Porous Medium Modeling

By a simple one-dimensional energy balance (Generalized Bernoulli´s equation) between upstream and downstream the porous medium and using Darcy´s pressure it is possible to derive the equivalent permeability of the anti-debris screen as:

$$\Delta p = \frac{\rho K C^2}{2} = \frac{\mu \Delta x C}{\kappa} \Rightarrow \kappa = \frac{2\mu\Delta x}{\rho K C} \tag{13}$$

where:

κ = permeability; ρ = density; K = accessory loss factor; *C* = fluid mean velocity; Δx = width of porous medium; μ = dynamic viscosity

Then, a restrictive body force is added into the RANS equations as:

$$B = R_c U \tag{14}$$

where, according to eqn. 13:

$$R_c = \frac{\mu}{\kappa} = \frac{\rho K C}{2\Delta x} \tag{15}$$

The porosity γ is imposed as a fraction of the cell volume V' open to the flow with respect to whole cell volume V. γ varies between 0 and 1.

$$V' = \gamma V \tag{16}$$

NUMERICAL ANALYSIS

Three meshes of 96290, 113884 and 120568 hexaedrals respectively, were analyzed. From a thorough comparison (Arévalo, 2004) the 113884-element mesh was selected. A typical simulation took around 10.000 iterations for a complete convergence, starting from a previously converged case. Every simulation took about 7 days running on a Pentium III PC.

Most of the following results represent a reservoir free-surface at 240 a.s.l. (prototype level) and a penstock flow velocity of 0.95 m/s, i.e., a flow-rate of 0.0914 m^3/s (equivalent to 450 m^3/s in the prototype). The anti-debris screen was modeled as indicated in the previous section, with porosity of 54% and Rc = 2727 kg/m^3seg. Fig. 2 shows a comparison of the velocity profile just downstream the location of the anti-debris screen at the duct mid-height with and without the porous medium to compare the effects. The velocity profile on each side of the mid/vane depicts a more restricted but uniform flow with the presence of the screen (porous medium).

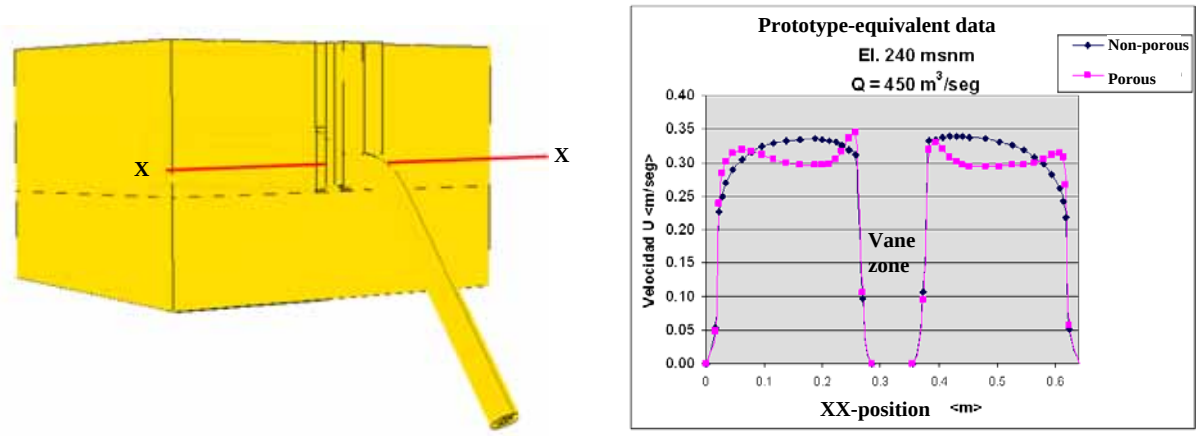

Fig. 2 Computational Model and boundary conditions

The computed pressure head is compared to experimental data taken along the penstock using open pressure gauges. For comparison purposes, pressure data is taken along the lines indicated in Fig. 3.

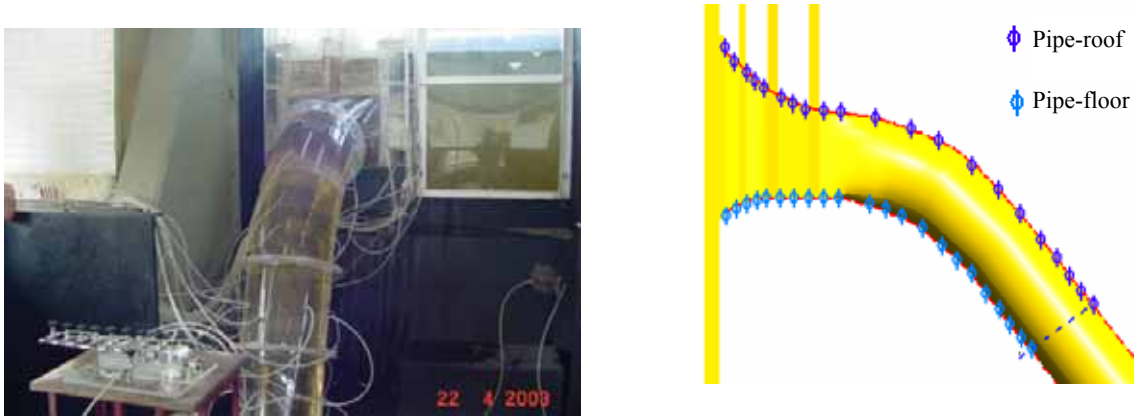

Fig. 3 Lines of pressure (experimental/numerical) gauge stations

Pressure measurements along the upper and lower edges of the entrance section of the pipeline (penstock) is compared to numerical calculations for a model flow-rate of 0.28 m^3/s and a free-surface level at an equivalent prototype level of 235 a.s.l. Results, in Fig. 4, depict a very good agreement between computed results and experimental data. Pressure field behaves as expected: the initial flow-section reduction causes a velocity increase and therefore, the pressure drops along upper and lower edges as the flow approaches the penstock elbow. Thereafter, the elbow local centrifugal acceleration causes a pressure drop along the upper edge, while the opposite occurs along the lower edge (see Fig. 4).

Comparison of free-surface local levels along the penstock sluice gate slots is shown in Fig.5. The 3D nature of the CFD simulation tends to distort the free-surface across the sluice gate slot section; therefore, an average line is included in the plot to make it easy for the purpose of comparison with experimental data.

Results demonstrate an excellent agreement between predicted levels and experiments, with a difference around 2%.

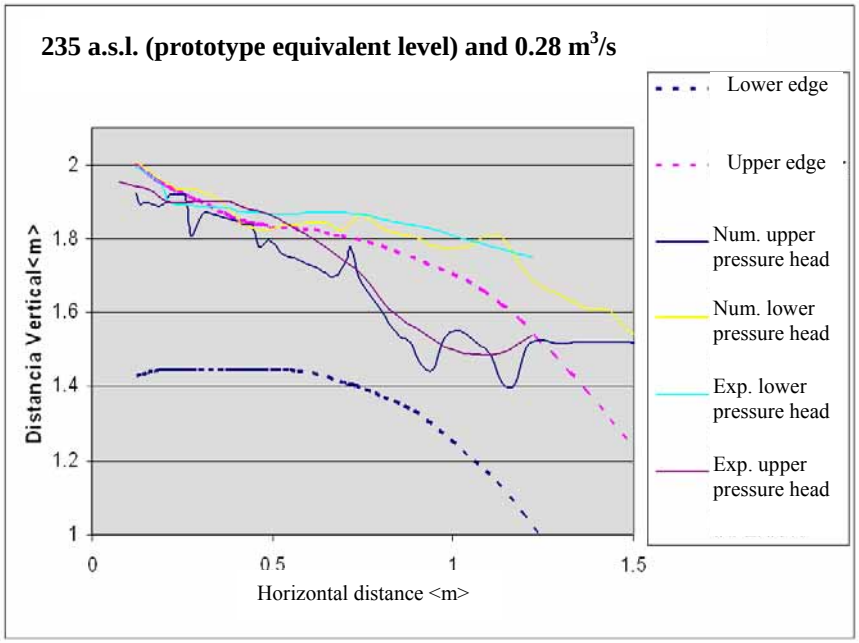

Fig. 4 Numerical pressure head vs. experimental data along penstock at 0.28 m3/s

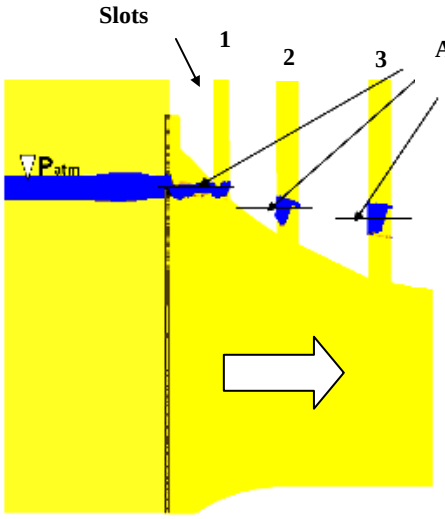

Height [m]	CFX	EXP	Error
Free surface	0.68	0.68	0%
Slot 1	0.63	0.66	3%
Slot 2	0.61	0.63	2%
Slot 3	0.60	0.62	2.%

Fig.5 Surface levels along the penstock sluice gate slots. Reservoir level of 235 a.s.l. (prototype equivalent level) and 0.091m^3/seg

As an additional contribution of this research, it was proposed an alternative approach to model the reservoir entrance. For the simple hydrostatic pressure boundary condition at the entrance, the streamlines towards the penstock intake, show and asymmetric distribution (Arévalo, 2004). In her work, Arévalo demonstrated that the effect of that asymmetric distribution does not affect significantly the velocity distribution in both sides of the center vane at the penstock intake. However, it is believed that in order to capture a more realistic flow behavior nearby the penstock intake, it is necessary to guarantee a uniform distribution of the flow approaching the dam. Therefore, the plane hydrostatic pressure load at the inlet boundary condition was compared with the case in which a porous medium models the rock wall at the reservoir entrance in the experimental facility. The geometry of the reservoir was enlarged to allocate the porous

rock and the permeability and porosity of this wall were empirically adjusted, taken advantage from the anti-debris screen modeling. Figure 6 shows the dimensions and location of the porous wall and the enlarged domain.

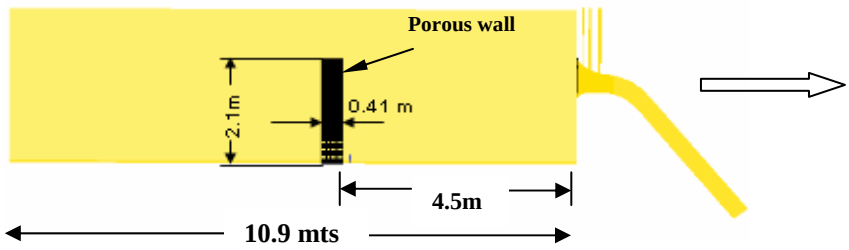

Fig. 6 Location and dimensions of porous medium at reservoir entrance

Top views of the streamlines for both cases are depicted in Fig. 7.

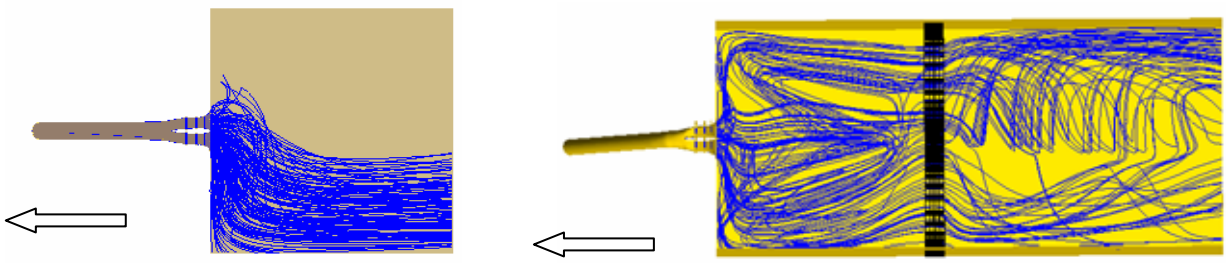

(a) **(b)**

Fig. 7 Top view of streamlines for 0.284 m^3/s and 235 a.s.l. (equivalent prototype level). (a) Without porous medium at entrance ; (b) With porous medium at entrance

Further evidence of the improvement in the modeling of the flow distribution approaching the penstock is shown in Fig. 8. The velocity distribution is largely more organized and uniform downstream the porous rock than upstream of it.

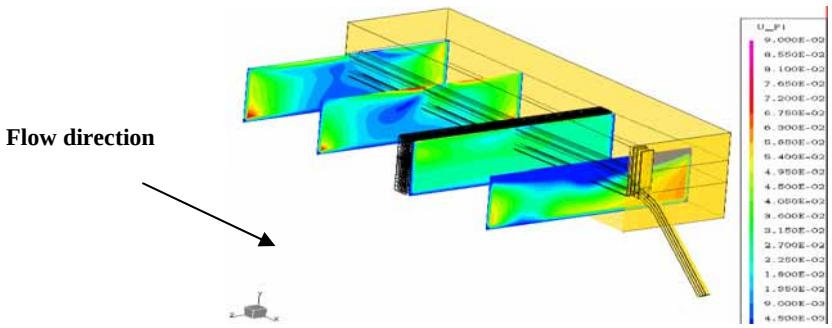

Fig. 8 Streamwise-velocity distribution upstream and downstream the porous wall for a typical flow condition.

CONCLUDING REMARKS

The comparison between numerical results and experimental data of the free surface flow within a 1:30 model of the intake (penstock) to Power House II of Guri Hydro-Power Plant (Venezuela) is presented.

The numerical model reproduced satisfactorily the pressure field and free-surface level observed in the experiments on the 1:30 model of one section of Guri's Powerhouse II. The proposed porous medium model for the anti-debris screen drew very good results and demonstrated that in future and more complex simulations, the screen and other high-flow resistance components within the free-surface model can be modeled as an equivalent porous medium.

The research also proved the convenience of using a porous wall at the entrance of the reservoir in order to facilitate the uniformity of the flow approaching the dam. Although the pressure condition is very robust for convergence purposes, it may cause distortion in otherwise expected symmetric flow distribution. In fact, the porous wall just reproduces the actual rock wall typically used in the experimental facility with the same purpose.

Results demonstrate the feasibility of extending the use of CFD for more complex studies, mostly oriented to 1:1 modeling.

REFERENCES

1. AEA Technology Engineering Software, Inc., "CFX - 4.4^{TM}. Solver Manual", 1997.
2. A. Arévalo "Validación de un modelo matemático en CFD para la simulación numérica en la entrada de la toma del modelo de las turbinas de la Represa del Guri", Proyecto de Grado, Coordinación de Ingeniería Mecánica, Universidad Simón Bolívar, Febrero 2004.
3. Patankar, S., "Numerical Heat Transfer and Fluid Flow", Ed. Hemisphere, New York, 1983.
4. Potter M. y Wiggerte D., Mecánica de Fluidos. Segunda Edición, 1998.
5. Streeter V. y Wylie B., Mecánica de Fluidos. Sexta Edición 1979.
6. Montilla, G., "Modelaje de Vórtices y Arrastre de Aire Para Condición de Sumergencia Crítica en la Central Hidroeléctrica de Guri", Tesis de Maestría en Ingeniería Hidráulica, Facultad de Ingeniería, Escuela de Ingeniería Civil, Universidad Central de Venezuela, Julio 2004.
7. CRS4 Technical Report 99/20, "Simulation of the Free Surface Flow inside a Rotating Cylinder", http://www.crs4.it/~cfdea/LMfreesurf/rotcyl.html, 1999